RSC Advances

ROYAL SOCIETY OF CHEMISTRY

www.rsc.org/advances

CdS Sensitized TiO_2 Photoanodes for Quantum Dot-Sensitized Solar Cells by Hydrothermal Assisted Chemical Bath Deposition And Post-Annealing Treatment†

Quanxin Zhang, Jiamei Cao, Hongguang Li*

Laboratory of Clean Energy Chemistry and Materials, Lanzhou Institute of Chemical Physics, Chinese Academy of Sciences, Lanzhou 730000, China

Abstract

A hydrothermal assisted chemical bath deposition method (HACBD) was proposed to directly deposit CdS quantum dots (QDs) on TiO_2 photoanodes in quantum dot-sensitized solar cells (QDSCs) for the first time. This method allows a facile and rapid growth and integration between CdS QDs and TiO_2 photanodes, with much lower cost compared to traditional chemical bath deposition (CBD). It was found the post-annealing temperature is crucial for the final performance of QDSCs. After proper annealing treatment, the conversion efficiency was enhanced from 1.52% to 1.78% under AM 1.5 illumination of 100 mW•cm^{-2}, which is attributed to the red shift of the absorption edge of CdS QDs and lower electron recombination rate at the photoanode/electrolyte interface.

Keywords: quantum dot-sensitized solar cells, hydrothermal method, chemical bath deposition, annealing treatment, power conversion efficiency

* Corresponding author: Prof. Dr. Hongguang Li E-mail: hgli@licp.cas.cn

Tel: +86-931-4968829 Fax: +86-931-4968163

1. Introduction

Quantum dot-sensitized solar cells (QDSCs) have been considered as promising next-generation solar cells due to their low cost and relatively high power conversion efficiency (PCE).[1-4] Quantum dots (QDs) show unique advantages over traditional dyes (such as Ru-polypyridine complexes and organic dyes) in dye-sensitized solar cells (DSCs) due to their strong photo-response in visible region, easily tunable bandgap and the expectation to obtain high PCE by utilizing multiple exciton generation of QDs.[5-7] Many efforts have been devoted to improving the performance and application in QDSCs, which can be mainly classified into four groups: 1) design and optimization of the method towards QDs growing on TiO_2 photoanodes; 2) optimization of the structure of the photoanodes; 3) surface treatment in photoanodes, such as annealing or ZnS passivation; 4) application of new kinds of QDs, electrolyte and counter electrodes.[8-14]

Among various factors influencing the quality of QDSCs, the QDs deposition method plays an important role, which determines the effective coverage of QDs on the surface of TiO_2 mesoporous film and the charge transfer efficiency between the interface of QDs and TiO_2.[2, 3] In general, two different deposition methods are adopted, i. e., 1) direct growth of QDs on TiO_2 film by chemical bath deposition (CBD) or by successive ionic layer adsorption and reaction (SILAR) and 2) attachment of pre-synthesized colloidal QDs to the electrode surface directly or with the aid of bifunctional linker molecules.[15, 16] These methods are sometimes combined in order to achieve co-sensitized deposition.[17] So far, highly effective QD coverage on TiO_2 mesoporous film as well as relatively better photovoltaic performance, was commonly obtained by the first method.[18] In addition, many studies have been devoted to exploring different assisted fabrication techniques, such as electrochemical deposition, photodeposition techniques and spray pyrolysis deposition.[19-22] Kuang *et*

al. adopted an *in situ* electrodeposition method to assemble CdS/CdSe co-sensitized solar cells, which presented 4.81% of efficiency with high short-circuit photocurrent density (J_{SC}) of 18.2 mA cm^{-2}.[23] Pan's group utilized microwave assisted CBD method to deposit CdS QDs on TiO_2 mesoporous film, which achieved a maximum short circuit current density of 7.20 mA cm^{-2} and a power conversion efficiency of 1.18% at one sun.[24]

Hydrothermal technique is a promising alternative deposition method because of the low processing temperature and the ease to control the particle size. The hydrothermal process has several advantages over others such as use of simple equipment, catalyst-free growth, low cost, large scale production, environmental friendliness and less hazardous.[25,26] However, up to now, hydrothermal technique is seldom studied to coat QDs onto TiO_2 photoanodes directly for QDSCs, although such a method has been applied in QDSCs for synthesizing QDs or fabricating ZnO nanowires as photoanodes.[27, 28]

In this work, a hydrothermal assisted chemical bath deposition (HACBD) method was adopted to directly deposit CdS QDs on TiO_2 photoanodes in QDSCs for the first time. HACBD avoids organic linker, repetitive immersing operation or high-temperature heating required in other methods, while the cells fabricated with HACBD achieved 1.52% of the efficiency, showing comparable conversion efficiency to those using other methods. Furthermore, it was found the post-annealing temperature is crucial for the final performance of QDSCs. After proper annealing treatment, the conversion efficiency was enhanced up to 1.78%, which is attributed to the red shift of the absorption edge of CdS QDs and lower electron recombination rate at the photoanode/electrolyte interface.

2. Experimental Section

Materials

Thiourea, $Cd(NO_3)_2$, Na_2S, sulfur were obtained from Sinopharm Chemical Reagent Co. Ltd. Ethyl cellulose (EC), terpineol, P25, 200 nm-sized anatase TiO_2 nanoparticles were purchased from Wuhan Jingge Solar Co. Ltd. All the chemicals were used without further purification. Solutions using for electrolyte and QDs deposition were prepared with high-purity water obtained from a water purification system (Ulupure Instrument Co. Ltd). The electrode substrate was fluorine-doped tin oxide conducting glass (FTO, thickness: 2.2 mm, Nippon, sheet resistance 14 Ω/square).

Preparation of CdS-coated photoanodes

A TiO_2 paste used for doctor-blading was prepared by using the mixture of P25 nanoparticles and 200 nm TiO_2 particles with the weight ratio of 6: 4, which was dispersed in terpineol with ethyl cellulose (the same proportion by weight) as a binder.[29] A 4-μm thick TiO_2 layer was coated on FTO glass using the TiO_2 paste. After that, TiO_2 layers were leveled for 15 min, then heated at 80 ℃ for 30 min, finally annealed at 450 ℃ for 30 min. TiO_2 films were further immersed in 40 mM $TiCl_4$ solution, rinsed, dried, and annealed at 500 ℃ in air for 30 min.[30]

CdS QDs were directly grown in the obtained TiO_2 film by top-down suspending the TiO_2 film in aqueous solution containing 2mM $Cd(NO_3)_2$ and 2mM thiourea, followed by sealing in an autoclave at 140 ℃ for 2 h. The photoanodes were rinsed with deionized water thoroughly and dried in air. Furthermore, for post-annealing treatment, as-prepared CdS-coated photoanodes were heated to 300 ℃, 400 ℃, 450 ℃ and 500 ℃ at 10 ℃·min^{-1} for 5 min, respectively. The as-prepared photoanode, and those annealed at 300 ℃, 400 ℃, 450 ℃ and 500 ℃ are denoted as Photoanode 1-5, respectively. For comparison, CdS-coated photoanodes with identical TiO_2 films were also prepared by using traditional CBD and SILAR method adopted in our previous articles.[4,31]

Characterization

The morphologies of as-prepared CdS-coated photoanodes were shown by transmission electron microscopy (TEM, JEOL JEM-100 CXII). Samples were prepared by scraping the photoanodes from the FTO substrate and dispersed in ethanol solution, followed by transferring several drops of the suspension onto a carbon-coated copper grid. The morphologies of CdS-coated photoanodes before and after annealing were investigated by scanning electron microscopy (SEM, JSM-6700F). XRD patterns of the CdS-coated photoanodes before and after annealing were measured between 20 and 80° in the 2θ scan mode using a Rigaku D/Max 2200-PC diffractometer with Cu Ka radiation (λ = 0.15418 nm) and a graphite monochromator at room temperature. The absorbance spectra of CdS coated photoanodes with different annealing temperature were recorded by UV-vis spectrophotometer (Shanghai Puyuan Instrument Co. Ltd).

Photocurrent density-photovoltage (*J*-*V*) measurements were measured in a sandwich structure solar cell with an active area of 0.20 cm^2. The polysulfide electrolyte was sandwiched between the CdS-coated TiO_2 film and the counter electrode to give the cell, which was separated by using a silicone spacer (thickness: 25 μm). The electrolyte contained 1M Na_2S and 1M S with a mixture solution of methanol and water (3/7, v/v). Cu_2S on copper was used as counter electrode fabricated according to the literature.[4] The cells were measured by a source meter (Keithley 2400) under an illumination of a solar simulator (SS150A, Zolix Instrument Co. Ltd.) under AM 1.5 illumination of 100 mW cm^{-2}. The incident-photon-to-current conversion efficiency (IPCE) was measured by DC method using an IPCE system (Solar Cell Scan 100, Zolix Instrument Co. Ltd.) without bias illumination. Electrochemical impedance spectra (EIS) was recorded in the sandwich cell using a CHI 600E electrochemical analyzer in dark. The measured frequency for EIS ranged from 100 mHz to 100 kHz and the amplitude was set to 10 mV. The results were fitted by Zview software.

3. Results and discussion

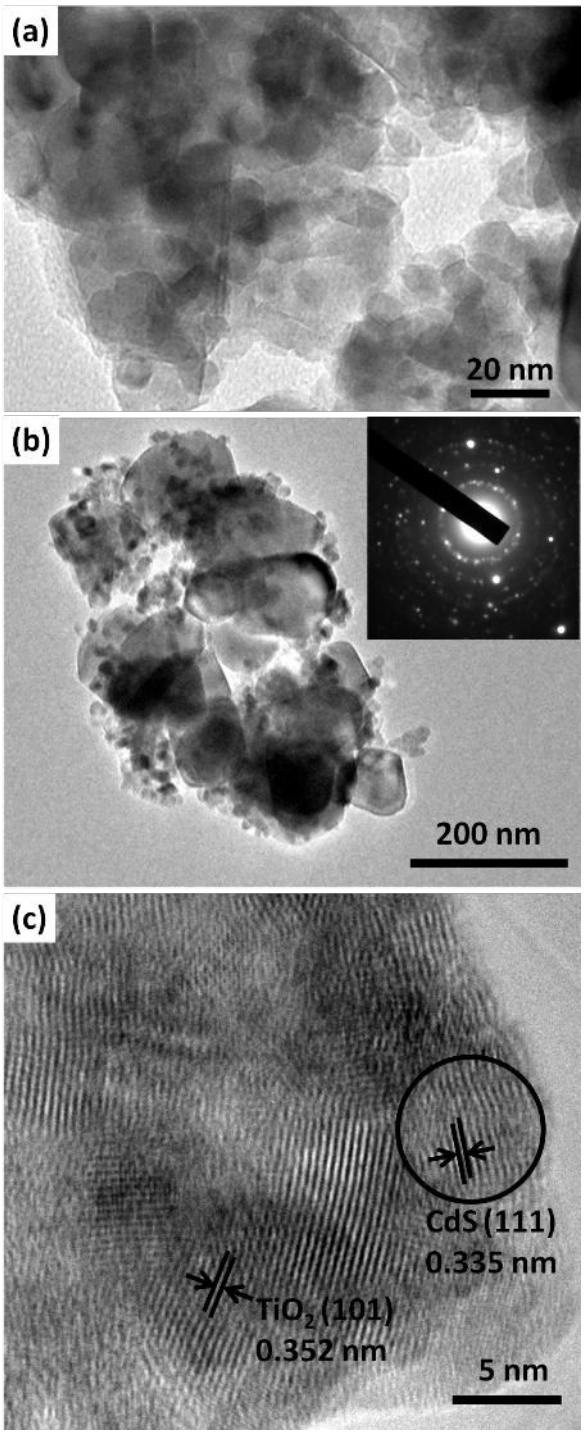

Fig. 1 a, b) TEM images of as-prepared CdS-coated photoanode (denoted as Photoanode 1) by HACBD in different magnification. Inset in b is the corresponding SAED pattern. c) HRTEM image of Photoanode 1. The circle marks the profile of CdS.

Fig. 1a shows a typical TEM image of as-prepared CdS-coated photoanode (Photoanode 1) by

HACBD method. It can be clearly seen that P25 nanoparticles in Photoanode 1 are in close contact to each other and form a mesoporous nanostructure. From the low-magnification TEM of Photoanode 1 in Fig. 1b, it is shown that the aggregates composed of P25 nanoparticles and TiO_2 particles with an average diameter of ~ 200 nm. CdS QDs are difficult to be observed in TEM images with low and medium magnifications. The corresponding selected area electron diffraction (SAED) pattern inset in Fig. 1b indicates that TiO_2/CdS film is a polycrystalline structure. Fig. 1c shows a high-resolution TEM (HRTEM) image of Photoanode 1. The lattice spacing of 0.352 nm is corresponding to the (101) plane of anatase TiO_2 (JCPDS 01-0562). The CdS cluster is composed of crystal grains with the average diameter of ~6.5 nm. The lattice spacing is determined to be 0.335 nm, which corresponds to the (111) plane of CdS (JCPDS 80-0019). Moreover, distinct lattice fringes in HRTEM images suggest good crystallinity of both TiO_2 and CdS.

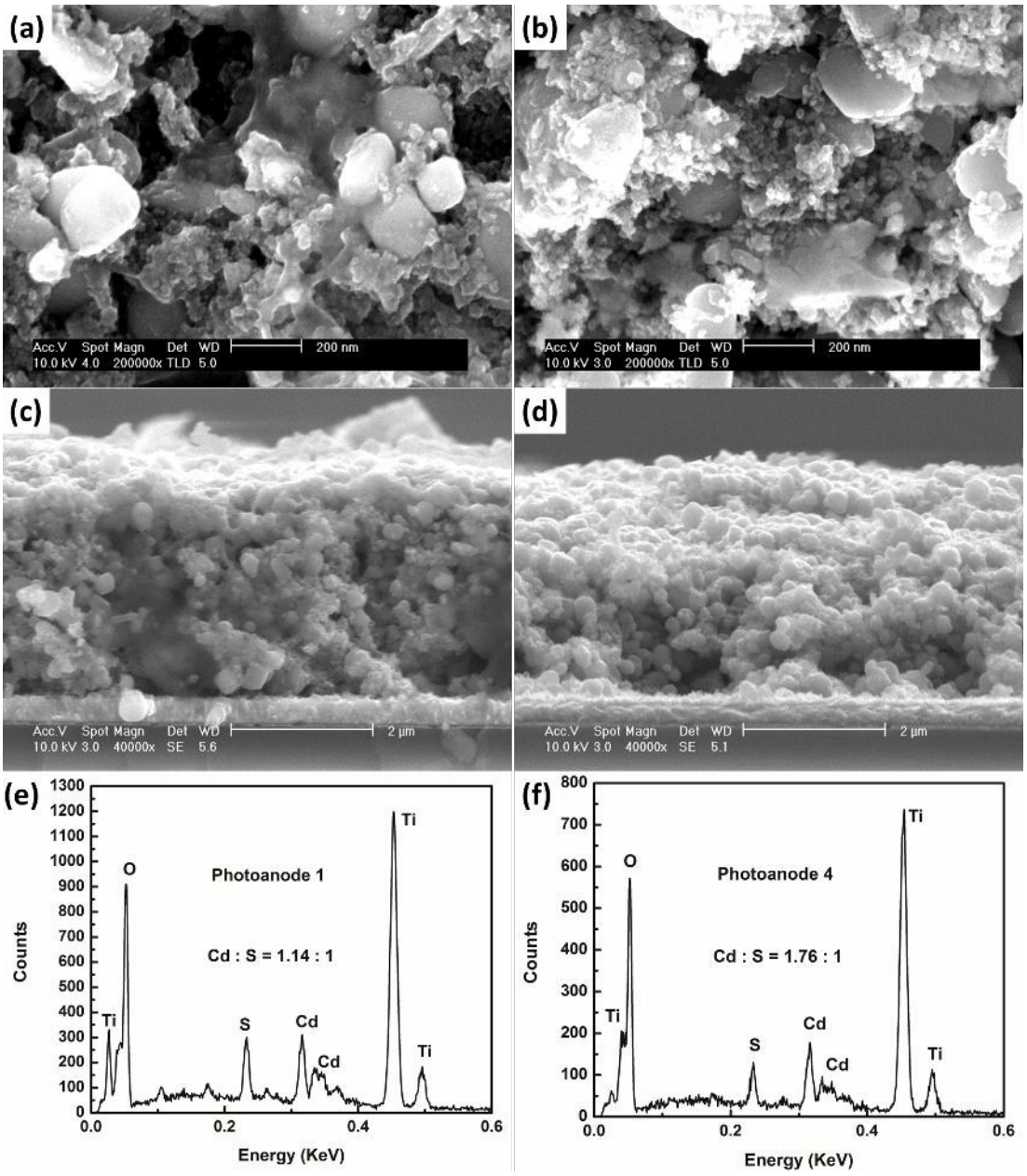

Fig. 2 SEM images showing the top (a, b) and side (c, d) views of CdS-coated photoanodes before (a, c Photoanode 1) and after annealing at 450 ℃ (b, d Photoanode 4). EDX spectra of Photoanode 1 (e) and 4 (f).

Fig. 2a and 2b show the top views of the photoanode before (Photoanode 1) and after (Photoanode 4) annealing at 450 ℃. The morphologies of Photoanode 2, 3 and 5 have also been examined and the results are summarized in Fig. S1. In all the cases, the mesopores are uniformly distributed in the films. A number of large pores exist around the TiO_2 particles (~200 nm), which

facilitate QDs growth without blocking the pores and electrolyte infiltration, demonstrating the advantage of using TiO_2 particles with the average diameter of ~200 nm in the fabrication of TiO_2 paste. Such structure can also favor the contact between the substrate and photoanode, enhancing the light scattering ability and improving the performance of the cells.[3,4] It can be seen clearly that some CdS aggregates appear in Photoanode 1. After annealing, most of the aggregates are sintered off as evidenced from Fig. 2c and 2d showing the side views of Photoanode 1 and 4, from which the thickness of the photoanodes was determined to be ~4μm. Fig. 2e and 2f present the identified composition of Photoanode 1 and 4 by energy dispersive X-ray spectroscopy (EDX) linked to SEM, respectively. The Cd : S atomic ratio in Photoanode 1 is about 1.14, demonstrating high-grade CdS particles formed. The Cd : S atomic ratio in Photoanode 4 increases to 1.76, indicating the S element has been sintered off. This result is in accordance with the SEM images shown above. It can be inferred that the annealing process contributes to removing redundant CdS aggregatesin photoanodes formed after HACBD. Fig. 3 shows the XRD patterns of Photoanode 1 and 4. Compared to Photoanode 1, the intensity of peaks corresponding to (111) and (220) planes of cubic phase CdS decrease in Photoanode 4, indicating a part of CdS is sintered off. The results are in agreement with the EDX data in Fig. 2. Besides, Photoanode 4 exhibits new peaks corresponding to (311) plane of CdO, inferring that a part of CdS transfers to CdO while annealing in air. Electrodes 2, 3 and 5 have similar XRD patterns to Photoanode 4, as shown in Fig. S2.

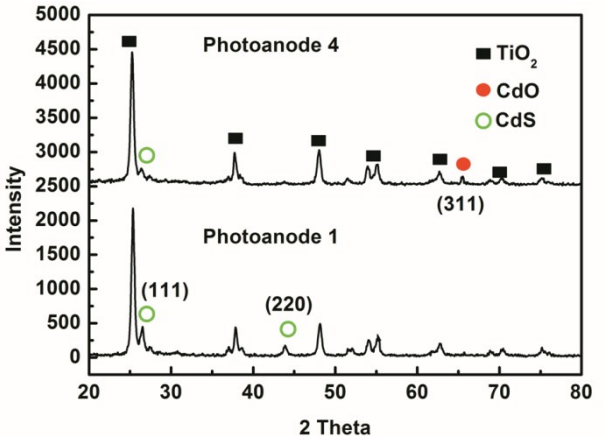

Fig. 3 XRD patterns of Photoanode 1 and 4, respectively.

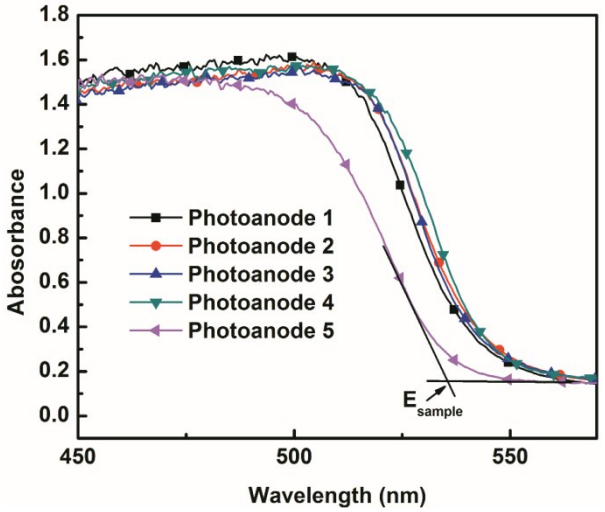

Fig. 4 UV-visible absorption spectra of CdS-coated TiO_2 electrodes with different annealing temperatures, which are denoted as Photoanode 1-5, respectively (for details, see the experimental section).

Fig. 4 presents a set of UV-visible absorption spectra of the CdS-coated TiO_2 electrodes versus different annealing temperatures. It is clearly shown that the absorption edge shifts toward longer wavelengths with increasing annealing temperature before 450 ℃ without serious decrease of the absorbance. The photon energy of the optical absorption shoulder point corresponds to the lowest excitation energy (E_{sample}) of the CdS QDs. The average diameter of the CdS QDs for each sintering temperature can be estimated by using Eq. (1) with an effective mass approximation, [32,33] where ΔE

is the band-gap shift, E_g is bulk band-gap energy, r is the QD radius, m_e, m_h, and m_0 are the effective electron mass, the hole mass, and the electron rest mass, respectively (m_e=0.13m_0, m_h=0.44m_0, and m_0=9.11*10^{-31} kg). The sizes of CdS particles from the excitonic peaks estimated for Phtoanode 1-4 are 6.5, 7.1, 7.3 and 7.8 nm, respectively. These results show that a higher annealing temperature triggers larger particle sizes of CdS nanocrystallites before 450 ℃, resulting in redshift of the absorption edge due to the size quantization effect. However, the decrease of absorbance and the obvious blueshift of the absorption edge is obtained for Photoanode 5 which was annealed at 500 ℃ in air, indicating that excessive CdS QDs have been sintered off at high temperature.

$$\Delta E = E_{sample} - E_g = \frac{hc}{\lambda_{sample}} - E_g = \frac{h^2}{8r^2}\left(\frac{1}{m_e} + \frac{1}{m_h}\right) \quad (1)$$

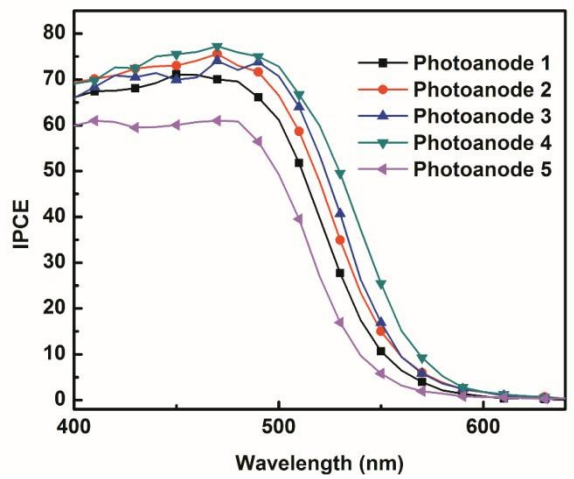

Fig. 5 IPCE spectra of CdS-sensitized QDSCs with different Photoanodes.

CdS decorated photoanodes are incorporated with Cu_2S counter electrode on brass and the S_2^{2-}/S^{2-} electrolyte into the QDSCs. Difference on IPCE versus Photoanodes 1-5 was first investigated. As can be seen from Fig. 5, variations of IPCE are consistent to the trends observed in UV-visible absorption shown in Fig. 4. IPCE values at 490 nm for Photoanodes 1-5 are 66%, 72%, 74%, 76% and 56%, respectively. Thus it can be concluded that when CdS annealing temperature is 450 ℃ (Photoanode 4), the QDSC exhibits the highest IPCE value which keeps ~75% in the

wavelength of 400-500 nm.

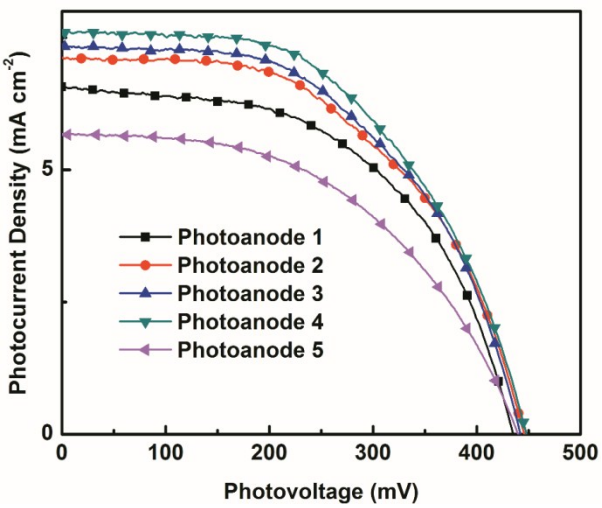

Fig. 6 *J-V* characteristics of CdS-sensitized QDSCs with different Photoanodes.

Table 1 Photovoltaic performance in QDSCs with different photoanodes.

Photoanode	J_{SC} (mA cm^{-2})	V_{OC} (mV)	FF	η (%)
1	6.57	435	0.53	1.52
2	7.12	444	0.52	1.65
3	7.32	442	0.52	1.69
4	7.60	448	0.52	1.78
5	5.68	440	0.50	1.24
CBD	6.45	399	0.51	1.31
SILAR	6.60	444	0.53	1.55

J-V characteristics for this series of CdS sensitized QDSCs are also given. As shown in Fig. 6 and Table 1, the QDSC without annealing can obtain a PCE (η) of 1.52%. Both J_{SC} and V_{OC} increase with increasing CdS annealing temperature, reaching maximum values of 7.60 mA cm^{-2} and 448 mV at an annealing temperature of 450 ℃. This yields the highest η of 1.78%. Obviously, with increasing annealing temperature, the sizes of CdS QDs increase, which generates more photo-excited electrons,

accounting for the higher J_{SC} and η of the device. However, when the annealing temperature was further increased to 500 ℃ (Photoanode 5), excessive CdS QDs are sintered off, causing a quick decrease of η. This is in coincidence with the IPCE results. In the mean time, varying annealing temperature on CdS-coated photoanodes does not make obvious difference on the fill factor (*FF*) of the QDSCs.

The effect of post-anealing treatment was further proven by the statistical results of *IV* data towards Photoanode 1 and Photoanode 4 for 10 times, respectively, as shown in Fig. S3. The fabrication and test conditions are the same for each time. Furthermore, the photovoltaic performances of QDSCs fabricated based on HACBD, traditional CBD and SILAR methods are compared (see Table 1). It can be observed that comparative J_{SC} and η values are achieved via HACBD without annealing compared with CBD and SILAR methods.

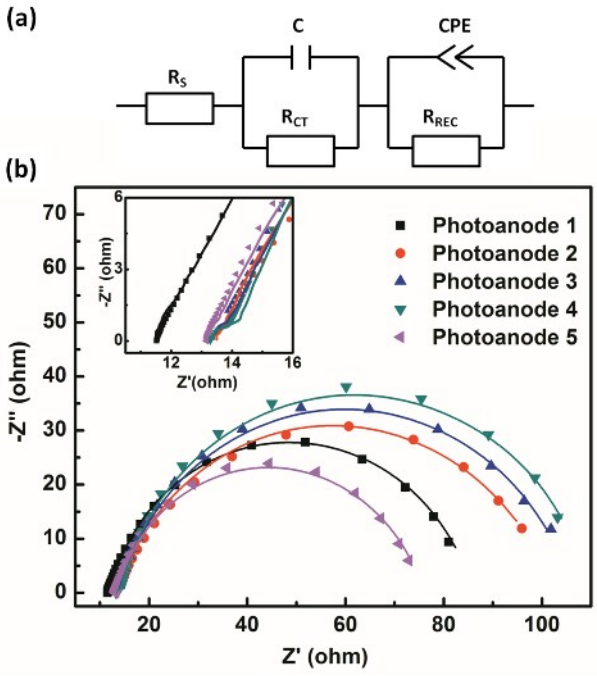

Fig. 7 a) Equivalent circuit for fitting EIS. b) Nyquist plots of the cells measured at zero bias potential in dark condition based on different photoanodes, the inset shows the abscissa expanded in the high frequency ranges. The scattered points are experimental data and the solid lines are the

fitting curves. R_S: series resistance; R_{CT} and C: charge transfer resistance and capacitance at the counter electrode/electrolyte interface in the high frequency ranges; R_{REC} and *CPE*: charge recombination resistance and constant phase element at the photoanode/electrolyte interface in the low frequency ranges.

It is known that the performance of the solar cell is influenced by its internal charge transfer significantly. Herein, EIS measurement in a sandwich cell was carried out to evaluate the electrochemical properties of phtoanodes with different annealing temperature on the cell performance.[34,35] The equivalent circuit for fitting EIS is shown in Fig. 7a. Fig. 7b presents typical Nyquist plots of the cells with different electrodes. Experimental curves are illustrated by symbols while the solid lines correspond to the fitted curves obtained with Zview software by using the equivalent circuit shown in the above of Fig. 7a. Two semicircles are obviously observed, the first small semicircle at high frequency reflects the charge transfer resistance (R_{CT}) and interfacial capacitance (C) at the counter electrode/electrolyte interfaces while the second large semicircle represents the charge recombination resistance (R_{REC}) and constant phase element (*CPE*) at the photoanode/electrolyte interface in the mid/low frequency range. Similar to the reported EIS results, no obvious response can be found toward the diffusion impedance of the redox species in the electrolyte, assigned to short circuit in the QDSC system.[36] In the high frequency (over 10^5 Hz), the ohmic series resistance (R_S) of the FTO layer, the electrode layer and the electrolyte can be determined where the phase is zero. The R_S, R_{CT}, and R_{REC} values are show in Table S1.

R_{CT} values for the QDSCs are all about 2 Ω·cm^2, indicating the counter electrodes and electrolyte are fabricated under the same condition. In our QDSCs, R_{REC} increases gradually from 74.0 to 96.3Ω·cm^2 in order of 0-450 ℃ CdS annealing temperature whereas decreases sharply at 500

℃ CdS annealing temperature. Obviously, increasing CdS annealing temperature will result in relatively low electron recombination rate between photogenerated electrons and S_2^{2-} at TiO_2/QDs/electrolyte interface. A possible explanation is that redundant CdS QDs formed in hydrothermal process are sintered off and the electron recombination centers decrease. However, excessive CdS QDs are sintered off at 500 ℃, resulting in more exposition of bare TiO_2 surface toward the S_2^{2-}/S^{2-} electrolyte and serious electrons recombination.[24,37]

Furthermore, the EIS spectra of QDSCs fabricated based on HACBD, CBD and SILAR methods are compared, in which R_{REC} is 74.0, 69.6 and 78.4, respectively (see Fig. S4 and Table S1). Although the cell with SILAR method exhibits a little lower electron recombination rate, the SILAR procedure is more complicated than CBD process. The cell with HACBD method has higher photovoltaic performance and lower electron recombination rate compared to that based on traditional CBD method. And it is worth mentioning that, the concentration of precursors for fabricating CdS QDs in HACBD is all 2 mM, which decreases by almost two orders of magnitude than those in traditional CBD and SILAR method.

4. Conclusions

In summary, we have demonstrated a simple, low-cost, and effective HACBD method to deposit CdS on TiO_2 photoanode directly for QDSCs for the first time. When assembled into QDSCs together with Cu_2S counter electrode and polysulfide electrolyte, the cell shows good performance with a J_{SC} of 6.57 mA cm^{-2} and η of 1.52%, which is comparative to the identical cells fabricated with traditional CBD and SILAR method. The photovoltaic performances of the cells with post-annealing treatment under different temperature are investigated. After proper annealing at 450 ℃, a maximum value of 1.78% conversion efficiency under one sun illumination has been achieved,

which is attributed to expanding the absorption edge of QDs and decreasing electron recombination rate at the photoanode/electrolyte interface while annealing. The hydrothermal assisted chemical bath deposition should be a promising fabrication technique for QDSCs.

Acknowledgments

This work was financially supported by the Hundred Talents Program of Chinese Academy of Sciences (Y20245YBR1) and National Natural Science Foundation of China (no. 21402215, no. 61474124).

Electronic Supplementary Information (ESI) available: SEM images and XRD patterns of Photoanode 2, 3 and 5, Nyquist plots of the cells based on photoanodes with different fabrication methods, EIS fitting data.

References

1. J.-H. Bang and P. V. Kamat, *ACS Nano* 2009, **3**, 1467-1476.

2. Y.-L. Lee and Y.-S. Lo, *Adv. Funct. Mater.* 2009, **19**, 604-609.

3. S. Giménez, I. Mora-Seró, L. Macor, N. Guijarro, T. Lana-Villarreal, R. Gómez, L. J. Diguna, Q. Shen, T. Toyoda and J. Bisquert, *Nanotechnology* 2009, **20**, 295204.

4. Q. X. Zhang, X. Z. Guo, X. M. Huang, S. Q. Huang, D. M. Li, Y. H. Luo, Q. Shen, T. Toyoda and Q. B. Meng, *Phys. Chem. Chem. Phys.*, 2011, **13**, 4659-4667.

5. C. Shen, L. D. Sun, Z. Y. Koh and Q. Wang, *J. Mater. Chem. A*, 2014, **2**, 2807-2813.

6. Y. P. Li, Y. Z. Hao, S. Sun, B. Sun, J. Pei, Y. H. Zhang, D. S. Xu and L. Liu, *RSC Adv.*, 2013, **3**, 1541-1546.

7. H. N. Chen, L. Q. Zhu, H. C. Liu and W. P. Li, *J. Phys. Chem. C*, 2013, **117**, 3739-3746.

8. I. Mora-Seró, S. Giménez, F. Fabregat-Santiago, R. Gómez, Q. Shen, T. Toyoda and J. Bisquert,

Acc. Chem. Res. 2009, **42**, 1848-1857.

9. C. Ratanatawanate, C. Xiong and Jr., K. J. Balkus, *ACS Nano*, 2008, 2, 1682-1688.

10. X. W. Zeng, W. J. Zhang, Y. Xie, D. H. Xiong, W. Chen, X. B. Xu, M. K. Wang and Y. B. Cheng, *J. Power Sources*, 2013, **226**, 359-362

11. G. Zhu, L. K. Pan, H. C. Sun, X. J. Liu, T. Lv, T. Lu, J. Yang and Z. Sun, *Chemphyschem*, 2012, **13**, 769-773.

12. Y. Q. Mao, Z. J. Zhou, T. Ling and X. W. Du, *RSC Adv.*, 2013, **3**, 1217-1221.

13. S. Peng, L. Tian, J. Liang, S. G. Mhaisalkar and S. Ramakrishna, *ACS Appl. Mater. Interfaces*, 2012, **4**, 397-404.

14. L. L. Li, P. N. Zhu, S. J. Peng, M. Srinivasan, Q. Y. Yan, A. S. Nair, B. Liu and S. Samakrishna, *J. Phys. Chem. C*, 2014, **118**, 16526-16535.

15. L. J. Diguna, Q. Shen, J. Kobayashi and T. Toyoda, *Appl. Phys. Lett.*, 2007, **91**, 023116.

16. O. Niitsoo, S. K. Sarkar, C. Pejoux, S. Rühle, D. Cahen and G. Hodes, *J. Photochem. Photobiol. A: Chem.*, 2006, **181**, 306-313.

17. I. Robel, V. Subramanian, M. Kuno and P. V. Kamat, *J. Am. Chem. Soc.*, 2006, **128**, 2385-2393.

18. S.-C. Lin, Y.-L. Lee, C.-H. Chang, Y.-J. Shen and Y.-M. Yang, *Appl. Phys. Lett.*, 2007, **90**, 143517.

19. S. Banerjee, S. K. Mohapatra, P. P. Das and M. Misra, *Chem. Mater.*, 2008, **20**, 6784-6791.

20. J. A. Seabold, K. Shankar, R. H. T. Wilke, M. Paulose, O. K. Varghese, C. A. Grimes and K. S. Choi, *Chem. Mater.*, 2008, **20**, 5266-5273.

21. Y. Jin-nouchi, S. Naya and H. Tada, *J. Phys. Chem. C*, 2010, **114**, 16837-16842.

22. Y. H. Lee, S. H. Im, J. H. Rhee, J. H. Lee and S. I. Seok, *ACS Appl. Mater. Interfaces*, 2010, **2**,

1648-1652.

23. X. Yu, J. Liao, K. Qiu, D. Kuang and C. Su, *ACS Nano*, 2011, **5**, 9494-9500.

24. G. Zhu, L. Pan, T. Xu and Z. Sun, *ACS Appl. Mater. Interfaces*, 2011, **3**, 1472-1478.

25. S. Baruah and J. Dutta, *Sci. Technol. Adv. Mater.*, 2009, **10**, 013001.

26. K. H. Tam, A. B. Djurisic, C. M. N. Chan, Y. Y. Xi, C. W. Tse, Y. H. Leung, W. K. Chan, F. C. C. Leung and D. W. T. Au, *Thin Solid Films*, 2008, **516**, 6167-6174.

27. H. Y. Li, M. Eastman, R. Schaller, W. Hudson and J. Jiao, *J. Nanosci. Nanotech.*, 2011, **11**, 8517-8521.

28. Q. Zhang, G. Chen, Y. Yang, X. Shen, Y. Zhang, C. Li, R. Yu, Y. Luo, D. Li and Q. Meng, *Phys. Chem. Chem. Phys.*, 2012, **14**, 6479−6486.

29. S. Ito, P. Chen, P. Comte, M. K. Nazeeruddin, P. Liska, P. Péchy and M. Grätzel, *Prog. PhotoVoltaics Res. Appl.*, 2007, **15**, 603–612.

30. Q. Zhang, S. Zhou, Q. Li and H. Li, *RSC Adv.*, 2015, **5**, 30617-30623.

31. Q. Zhang, Y. Zhang, S. Huang, X. Huang, Y. Luo, Q. Meng and D. Li, *Electrochem. Commun.*, 2010, **12**, 327-330.

32. W. W. Yu, L. Qu, W. Guo and X. Peng, *Chem. Mater.*, 2003, **15**, 2854-2860.

33. Q. Shen, J. Kobayashi, L. J. Diguna and T. Toyoda, *J. Appl. Phys.*, 2008, **103**, 084304.

34. N. Papageorgiou, *Coord. Chem. Rev.*, 2004, **248**, 1421−1446.

35. A. Hauch and A. Georg, *Electrochim. Acta*, 2001, **46**, 3457−3466.

36. V. González-Pedro, X. Q. Xu, I. Mora-Seró and J. Bisquert, *ACS Nano*, 2010, **4**, 5783-5790.

37. N. Guijarro, T. Lana-Villarreal, I. Mora-Seró, J. Bisquert and R. Gómez, *J. Phys. Chem C*, 2009, **113**, 4208-4214.

Graphical abstract

A hydrothermal assisted chemical bath deposition method was adopted to directly deposit CdS quantum dots on TiO_2 photoanodes in QDSCs for the first time. An efficiency of 1.78% is achieved with proper post-anealing treatment.